FEB 23 2000

SANDIA REPORT

SAND99–0631
Unlimited Release
Printed March 1999

RECEIVED
MAR 01 2000
OSTI

Modeling the Responses of TSM Resonators Under Various Loading Conditions

Helen L. Bandey, Stephen J. Martin, Richard W. Cernosek, and A. Robert Hillman

Prepared by
Sandia National Laboratories
Albuquerque, New Mexico 87185 and Livermore, California 94550

Sandia is a multiprogram laboratory operated by Sandia Corporation, a Lockheed Martin Company, for the United States Department of Energy under Contract DE-AC04-94AL85000.

Approved for public release; further dissemination unlimited.

Sandia National Laboratories

Issued by Sandia National Laboratories, operated for the United States Depart-ment of Energy by Sandia Corporation.

NOTICE: This report was prepared as an account of work sponsored by an agency of the United States Government. Neither the United States Govern-ment, nor any agency thereof, nor any of their employees, nor any of their contractors, subcontractors, or their employees, make any warranty, express or implied, or assume any legal liability or responsibility for the accuracy, completeness, or usefulness of any information, apparatus, product, or process disclosed, or represent that its use would not infringe privately owned rights. Reference herein to any specific commercial product, process, or service by trade name, trademark, manufacturer, or otherwise, does not necessarily constitute or imply its endorsement, recommendation, or favoring by the United States Government, any agency thereof, or any of their contractors or subcontractors. The views and opinions expressed herein do not necessarily state or reflect those of the United States Government, any agency thereof, or any of their contractors.

Printed in the United States of America. This report has been reproduced directly from the best available copy.

Available to DOE and DOE contractors from
Office of Scientific and Technical Information
P.O. Box 62
Oak Ridge, TN 37831

Prices available from (703) 605-6000
Web site: http://www.ntis.gov/ordering.htm

Available to the public from
National Technical Information Service
U.S. Department of Commerce
5285 Port Royal Rd
Springfield, VA 22161

NTIS price codes
Printed copy: A03
Microfiche copy: A01

DISCLAIMER

Portions of this document may be illegible in electronic image products. Images are produced from the best available original document.

SAND99-0631
Unlimited Release
Printed March 1999

Modeling the Responses of TSM Resonators under Various Loading Conditions

Helen L. Bandey,* Stephen J. Martin and Richard W. Cernosek
Microsensors Research and Development Department
Sandia National Laboratories
P.O. Box 5800
Albuquerque, NM 87185-1425

A. Robert Hillman
Chemistry Department
Leicester University
Leicester, LE1 7RH, UK

ABSTRACT

We develop a general model that describes the electrical responses of thickness shear mode resonators subject to a variety of surface conditions. The model incorporates a physically diverse set of single component loadings, including rigid solids, viscoelastic media, and fluids (Newtonian or Maxwellian). The model allows any number of these components to be combined in any configuration. Such multiple loadings are representative of a variety of physical situations encountered in electrochemical and other liquid phase applications, as well as gas phase applications. In the general case, the response of the composite load is not a linear combination of the individual component responses. We discuss application of the model in a qualitative diagnostic fashion to gain insight into the nature of the interfacial structure, and in a quantitative fashion to extract appropriate physical parameters such as liquid viscosity and density, and polymer shear moduli.

KEYWORDS

Thickness-shear mode resonator; quartz crystal microbalance; viscoelasticity; polymers; fluids; thin films.

---

* To whom correspondence should be addressed

INTRODUCTION

The thickness-shear mode (TSM) resonator, also known as the quartz crystal microbalance (QCM), and its electrochemical variant the EQCM are now mature techniques, routinely used to provide a wealth of thermodynamic and kinetic information on interfacial processes, in the latter case occurring under electrochemical potential control. In the simplest situation (that of a rigidly coupled film), the EQCM functions as a gravimetric probe of surface populations. However, it is increasingly recognized that many systems of interest - notably polymers - do not conform to this requirement. A number of publications (reviewed below) have considered isolated examples of cases that fall outside the "rigidly coupled film" scenario, and the topic has attracted considerable debate.[1] The purpose of this paper is to initiate a unified treatment ultimately capable of handling all physical circumstances likely to be encountered. This includes rigid and viscoelastic films, of finite or infinite extent, and fluids. Furthermore, we address the practically important situation that the resonator is loaded with more than one type of layer, as is almost invariably the case in an in situ electrochemical experiment. To our knowledge, a general model with these capabilities has not previously been described.

Characterization of thin films, rigidly coupled to the surface of quartz thickness-shear mode (TSM) resonators, is a well understood process. Frequency changes (Δf) of the resonator upon addition of mass can be directly related to the areal mass density (Δm) via the Sauerbrey equation:[2]

$$\Delta f = -\left(\frac{2}{\rho_q v_q}\right)\Delta m f_0^2 \qquad (1)$$

where ρ_q and v_q are the quartz density and wave velocity, respectively, (Table 1) and f_0 is the frequency of the unperturbed device. The Sauerbrey equation has been used very successfully for almost forty years to describe a wide range of "rigid film" situations. Initially, it was used to interpret TSM resonator data in solid/gas phase situations, typified by "thickness monitors" for metal deposition. This approach has subsequently formed the basis for the interpretation of TSM resonator data associated with the deposition and subsequent manipulation of a wide variety of films at the resonator surface.

Initially it was believed that the addition of a liquid to one side of the quartz resonator would result in excessive energy loss to the solution from viscous effects, to the extent that the

crystal would cease to oscillate. In 1980 Nomura et al.[3] were first to prove this incorrect, demonstrating that the TSM resonator had potential applications for chemical sensors in the liquid phase. This capability opened up the door to a wide range of in situ studies, including measuring properties of the contacting solution. Most notable among these developments was the electrochemical quartz crystal microbalance (EQCM) where one of the resonator electrodes is used as the working electrode in a conventional three-electrode electrochemical cell.[4-6]

Today, many of the materials studied on acoustic wave devices are not rigidly coupled to the electrode surface. For example, polymers, whose range of useful physical and chemical properties promise many potential applications, may show viscoelastic behavior. In the electrochemical context, materials are studied and applied in situ, i.e., exposed to solution, in which case films on the EQCM may not exhibit rigid behavior. The Sauerbrey approximation was not intended or envisaged to cover such situations, so its application requires appreciable care.

Crystal impedance is a technique that gives information on the deviations from rigidity of surface-bound films. It involves using an impedance analyzer to determine the spectrum over a specified frequency range in the vicinity of crystal resonance. By comparing the shape of the spectrum of the perturbed resonator to that of the unperturbed device, one can explore the validity of the Sauerbrey approximation. A translation towards lower frequency with no change in the shape of the spectrum is characteristic of a rigidly coupled mass layer. However, damping of the signal is characteristic of a lossy material, e.g., fluid or viscoelastic material.

Quantitatively, one can study crystal impedance data by using equivalent circuit analysis in which the electrical output of the resonator is subsequently related to the mechanical properties of the surface perturbation. Recently, use of equivalent circuit analysis to probe the resonator's electrical properties has opened up a new avenue of enquiry, yielding information on the physical properties of not only rigid mass layers, but also viscoelastic layers and liquids.[7-16] In this paper we present a general model for describing the physical properties of a range of chemically and physically distinct systems on the surface of a TSM resonator. Unlike previous treatments, we extend the models to multi-layer systems, showing how physical parameters can be obtained for each individual layer. This allows us to describe almost any system on the TSM resonator and extract relevant physical parameters.

THEORY

The TSM resonator consists of a thin disk of AT-cut quartz with metal electrodes deposited on both faces (Figure 1). Owing to the piezoelectric properties and crystalline orientation of the quartz, the application of an external electrical potential between these electrodes produces an internal mechanical stress and consequently a shear deformation of the crystal. If an alternating electric field is induced perpendicular to the surface of the crystal, the deformation will oscillate at the frequency of the applied field. The maximum amplitude of vibration occurs at the mechanical resonant frequency of the crystal (this corresponds to a crystal thickness that is an odd multiple of half the acoustic wavelength). If a medium contacts one or both of the resonator surfaces, the oscillating surface(s) interact mechanically with that medium. Owing to the electromechanical coupling that occurs in the quartz, the mechanical properties of the contacting medium are reflected in the electrical properties of the resonator. The object of this paper is to relate the electrical properties of the resonator to the mechanical properties of the contacting medium in order that the latter may be extracted from measurements of the former.

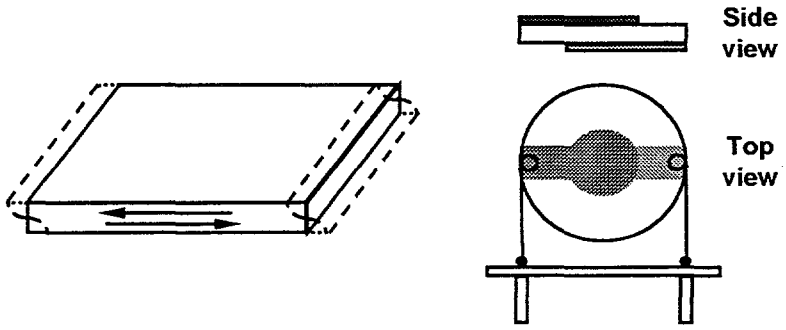

Figure 1. Electrode design for a typical TSM resonator.

A one-port electrical device is characterized by its input electrical impedance, Z, measured over a range of excitation frequencies, f. In practice, this is commonly accomplished using an impedance analyzer that excites the TSM resonator with a controlled amplitude incident voltage and measures the reflected signal over a range of frequencies around crystal resonance. The ratio of reflected to incident voltages is denoted by the scattering parameter S_{11}; this is a complex quantity, representing both the magnitude ratio and phase relation between the incident and reflected signals. The input impedance is found from S_{11} by[17]

$$Z(f) = Z_0\left(\frac{1+S_{11}(f)}{1-S_{11}(f)}\right) \tag{2}$$

where Z_0 is the characteristic impedance of the measurement system (typically 50 Ω).

Transmission-Line Model. The most accurate electrical representation to date for a piezoelectric bulk-wave resonator is given by the transmission-line model based on a three-port Mason model (Figure 2).[17, 18] There are two acoustic ports that represent the two crystal faces. These acoustic ports are connected by a transmission-line that represents the phase shift and loss experienced by an acoustic wave propagating across the quartz thickness. A 1:*N* transformer, representing the electromechanical coupling between the applied voltage (at *A*-*B*) and quartz shear displacement (at *C*-*D*), couples the acoustic ports to the electrical port.

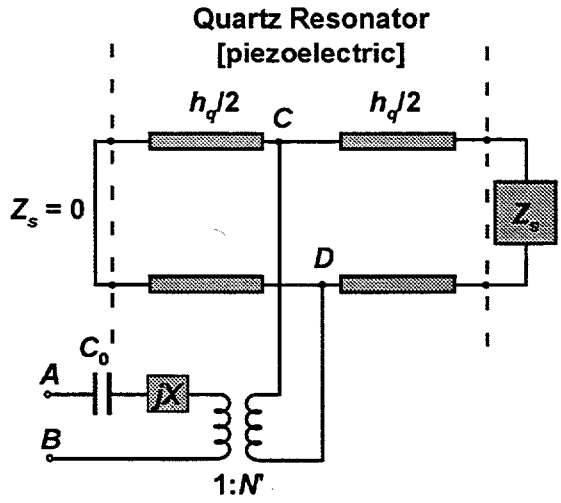

Figure 2. Transmission-line representation[19] of a TSM resonator with one stress-free and one loaded surface.

Mechanical loading of the quartz resonator is represented by a mechanical impedance, Z_s, which is the ratio of surface stress to particle velocity at the device surface:

$$Z_s = \left.\frac{T_{xy}}{v_x}\right|_{y=0} \tag{3}$$

where T_{xy} is the sinusoidal steady-state shear stress (force per unit area in the x-direction on a y-normal plane) imposed on the contacting medium by the resonator, and v_x is the resulting x-directed surface shear particle velocity (Figure 3).

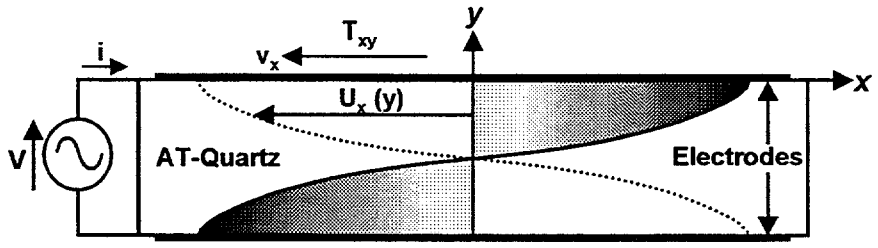

Figure 3. Cross-sectional view of an unperturbed TSM resonator where T_{xy} is the surface shear stress, v_x is the resulting particle velocity and u_x is the resulting particle displacement in the x-direction.

For the unperturbed quartz crystal, both of the surfaces may be considered as stress-free boundaries (neglecting electrode mass) which gives $Z_s = 0$, analogous to a short-circuit at both acoustic ports. In most sensing applications, one of the ports is unloaded and acts as a short circuit ($Z_s = 0$), while the other is terminated by a non-zero surface mechanical impedance, Z_s. The complex electrical input impedance for the quartz resonator described by the transmission-line model in Figure 2 is[8]

$$Z = Z_{AB} = \frac{1}{j\omega C_0} + jX + \frac{1}{(N')^2} Z_{CD} \tag{4}$$

where Z_{CD} is the complex mechanical impedance, $\omega = 2\pi f$ (f is the excitation frequency), X is the reactance of the piezoelectric interaction, N' is the transformer turn ratio representing the quartz electromechanical coupling, C_0 is the static capacitance of the resonator, and $j = (-1)^{½}$. Expressions for X and N' are defined in the literature.[20] Further development of transmission-line components leads to[8]

$$Z_{AB} = \frac{1}{j\omega C_0}\left[1 - \frac{K^2}{\phi_q}\frac{2\tan(\phi_q/2) - j(Z_s/Z_q)}{1 - j(Z_s/Z_q)\cot(\phi_q)}\right] \tag{5}$$

where K^2 is the complex electromechanical coupling factor for lossy quartz (Table 1), ϕ_q is the complex acoustic phase shift across the lossy quartz, and Z_q is the quartz characteristic impedance ($Z_q = (\rho_q \mu_q)^{½}$ where μ_q is the quartz shear elastic constant (Table 1)). The electrical impedance in eq 5 can be represented as a motional impedance, Z_m (arising from mechanical motion), in parallel with C_0 as [8, 19]

$$Z_m = \frac{1}{j\omega C_0}\left[\frac{\phi_q/K^2}{2\tan(\phi_q/2)} - 1\right] + \frac{\phi_q(Z_s/Z_q)}{4K^2\omega C_0}\left[1 - \frac{j(Z_s/Z_q)}{2\tan(\phi_q/2)}\right]^{-1} \tag{6}$$

The first term in eq 6 represents the motional impedance for the unperturbed resonator (Z_m^0), while the second term represents the motional impedance created by the surface load (Z_m^1).

Permittivity, ε_q ($A^2\ s^4\ g^{-1}\ cm^{-3}$)	3.982×10^{-13}
Viscosity, η_q ($g\ cm^{-1}\ s^{-1}$)	3.5×10^{-3}
Shear elastic constant, μ_q ($dyne\ cm^{-2}$)	2.947×10^{11}
Density, ρ_q ($g\ cm^{-3}$)	2.651
Electro mechanical coupling factor, K^2	7.74×10^{-3}
Wave velocity, v_q ($cm\ s^{-1}$)	3.34×10^5

Table 1. Properties of AT-cut quartz.[21]

The Unperturbed Resonator. For an unperturbed resonator operating at frequencies near the mechanical resonance ($\phi \cong N\pi$), the transmission-line model can be simplified to get an expression in terms of lumped-elements. By using the identity $\tan(\phi_q/2) = 4\phi_q/[(N\pi)^2 - \phi_q^2]$ and $\phi_q^2 = [(N\pi)^2 - 8K^2]/(1 + j\xi)$ where $\xi = \omega\eta_q/\mu_q$, and assuming that $8K^2 \ll (N\pi)^2$ and $\omega = \omega_s$, the first term in eq 6 can be approximated as[10]

$$Z_m^0 = \frac{1}{j\omega C_0}\left[\frac{\phi_q/K^2}{2\tan(\phi_q/2)} - 1\right] \approx R_1 + j\omega L_1 + \frac{1}{j\omega C_1} \tag{7}$$

where η_q is the effective viscosity for quartz (Table 1), $\omega_s = 2\pi f_s$ where f_s is the series resonant frequency for the unperturbed TSM resonator, and N is the resonator harmonic number. This approximation describes the motional impedance for the Butterworth-Van Dyke (BVD) equivalent circuit of an unperturbed resonator (Figure 4a with $Z_m^1 = 0$). It has been shown previously that this simpler lumped-element model can be used instead of the transmission-line representation, and the deviation between the models is negligible for the unperturbed resonator.[19]

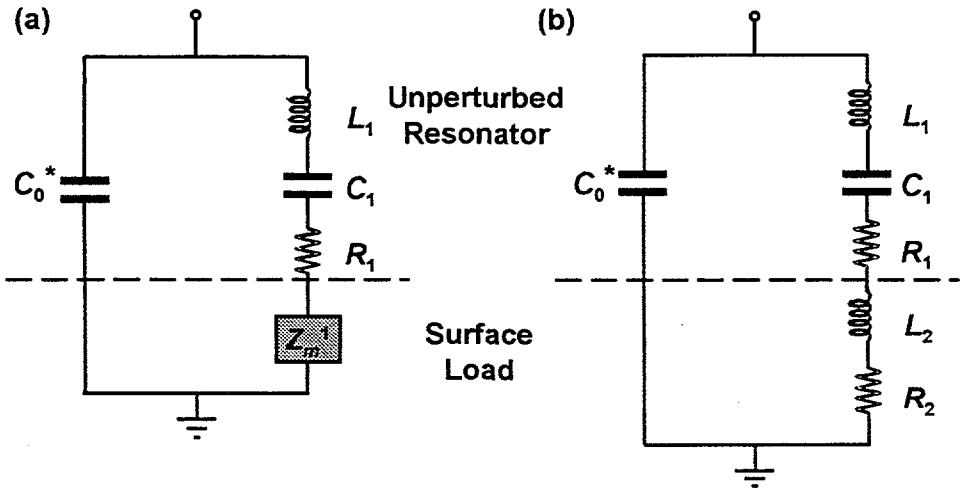

Figure 4. Modified Butterworth-Van Dyke equivalent circuit with (a) a complex surface impedance element, Z_m^1, and (b) a motional inductance, L_2, and resistance, R_2.

The BVD model consists of a "static" and "motional" arm in parallel. The static arm consists of a capacitance, C_0*, where

$$C_0^* = C_0 + C_p \tag{8}$$

C_p is the parasitic or stray capacitance, external to the quartz, due to the geometry of the test fixture and electrode pattern. The motional arm, containing L_1, C_1 and R_1, arises due to the electromechanical coupling of piezoelectric quartz (i.e., due to the motion of the resonating crystal). The capacitive component, C_1, represents the mechanical elasticity of the system; the inductive component, L_1, represents inertial mass changes; and the resistive component, R_1, represents dissipation of energy due to viscous effects, internal friction, and damping from the crystal mounting. The static capacitance, C_0*, dominates the admittance (reciprocal of impedance) away from resonance, while the motional contribution dominates near resonance. The elements of the equivalent circuit for the unperturbed resonator are given by[10]

$$\mathrm{C}_0 = \frac{\varepsilon_q \mathrm{A}}{\mathrm{h}_q} \tag{9}$$

$$C_1 = \frac{8K^2 C_0}{(N\pi)^2} \tag{10}$$

$$L_1 = \frac{1}{\omega_s^2 C_1} \tag{11}$$

$$R_1 = \frac{\eta_q}{\mu_q C_1} \tag{12}$$

where ε_q is the permittivity for quartz (Table 1), A is the effective electrode area, and h_q is the quartz crystal thickness.

The Surface Loaded Resonator. A load on the surface of a resonator can be represented by a surface mechanical impedance, Z_s (eq 3). This is shown for the transmission-line model in Figure 2. Similarly, the lumped-element model is modified with a motional impedance, Z_m^1, as shown in Figure 4a. Z_s is a complex quantity: the real part, Re(Z_s), corresponds to the component of surface stress in phase with the surface particle velocity and represents mechanical power dissipation at the surface; the imaginary part, Im(Z_s), corresponds to the stress component 90° out-of-phase with particle velocity and represents mechanical energy storage at the surface.

The transmission-line model is the more accurate of the two models since it imposes no restrictions on the surface mechanical load impedance. However, the lumped element approach is easier to visualize and often requires less effort to extract parameters. It has been shown[19] that, in all cases, the relative deviations in the resonator parameters (Δf and ΔR) computed by the two models does not exceed 3% for most practical loading conditions operating at the resonator fundamental frequency. Theoretically, if the ratio of Z_s to Z_q does not exceed 0.1, the lumped-element model always predicts responses within 1% of those for the transmission-line model. Thus the motional impedance created by a surface load (described by the second term in eq 6) can be approximated by

$$Z_m^1 = \frac{\phi_q(Z_s/Z_q)}{4K^2\omega C_0}\left[1 - \frac{j(Z_s/Z_q)}{2\tan(\phi_q/2)}\right]^{-1} \approx \frac{N\pi}{4K^2\omega_s C_0}\left(\frac{Z_s}{Z_q}\right) \tag{13}$$

Furthermore, Z_m^1 is complex and can be separated into real and imaginary components (see Figure 4b):

$$Z_m^1 = R_2 + j\omega L_2 \tag{14}$$

The equivalent circuit parameters, R_2 and L_2, can be related to Z_s by

$$R_2 = \frac{N\pi}{4K^2\omega_s C_0}\frac{\mathrm{Re}(Z_s)}{Z_q} \tag{15}$$

and

$$X_2 = \omega L_2 = \frac{N\pi}{4K^2\omega_s C_0}\frac{\mathrm{Im}(Z_s)}{Z_q} \tag{16}$$

Eq 7 can be modified to give the total motional impedance, described by the lumped-element model, for a surface-loaded resonator:

$$Z_m = (R_1 + R_2) + j\omega(L_1 + L_2) + \frac{1}{j\omega C_1} \tag{17}$$

PERTURBATIONS ON THE TSM RESONATOR

There are three primary surface load types that can be applied to a quartz resonator: an ideal mass layer, a fluid, and a viscoelastic medium. The first two are special cases of the latter. Addition of these layers to the resonator surface will present different surface mechanical impedances, and hence change the electrical characteristics of the system. This section relates Z_s to the physical parameters of the different surface loads, not only for single-layered, but also for multi-layered and semi-infinite systems. The different systems studied are summarized in Table 2 at the end of the section. The list is not exhaustive, but the cases presented describe the majority of single/multi-layered systems likely to be encountered on the TSM resonator.

Ideal Mass Layer. A film that is sufficiently thin and rigid so that there is negligible acoustic phase shift, ϕ, across the layer thickness may be approximated as an ideal mass layer, i.e., one that is infinitesimally thin, yet imposes a finite mass per unit area on the resonator surface. In this case the entire layer moves synchronously with the quartz surface (Figure 5).

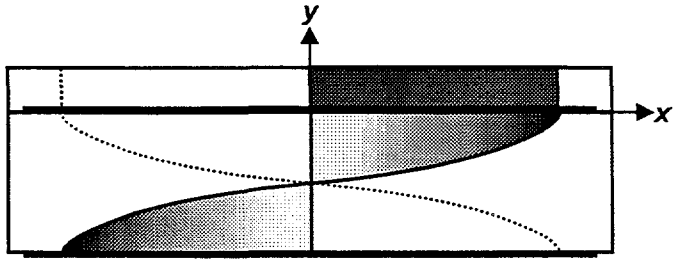

Figure 5. Cross-sectional view of a TSM resonator with a layer behaving as an ideal mass layer on the upper surface. The acoustic phase shift across the layer is negligible.

The surface stress, T_{xy}, required to sinusoidally accelerate a mass layer is

$$T_{xy} = \rho_s \dot{v}_{xo} \tag{18}$$

where v_{xo} is the surface particle velocity and $\dot{v}_{xo} = \partial v_{xo}/\partial t$. ρ_s is the mass per unit area contributed by the layer ($\rho_s = h_s \rho_{iml}$, where h_s and ρ_{iml} are the thickness and density of the ideal mass layer, respectively). For a sinusoidal oscillation

$$v_x = v_{xo} e^{j\omega t} \tag{19}$$

and

$$T_{xy} = j\omega v_{xo} \rho_s \tag{20}$$

The surface mechanical impedance, Z_s, associated with an ideal mass layer is obtained by combining eqs 3 and 20 to give

$$Z_s = j\omega\rho_s \tag{21}$$

Combining eq 21 with 15 and 16 gives the motional impedance elements arising from the ideal mass layer:[22]

$$R_2 = 0 \tag{22}$$

and

$$X_2 = \frac{N\pi}{4K^2\omega_s C_0}\frac{\omega\rho_s}{Z_q} \tag{23}$$

From eqs 22 and 23, it can be seen that there is no power dissipation (R_2), but only energy storage (X_2) arising from the kinetic energy of the mass layer. This energy storage is proportional to the surface mass density.

The unperturbed series resonant frequency, f_s, is defined as the frequency at which the motional reactance is zero, i.e.,

$$j\omega_s L_1 + \frac{1}{j\omega_s C_1} = 0 \tag{24}$$

Solving eq 24 for ω_s and noting that $\omega_s = 2\pi f_s$, gives

$$f_s = \frac{1}{2\pi(L_1 C_1)^{1/2}} \tag{25}$$

For the perturbed resonator with mass loading:

$$\Delta f_s \cong -\frac{L_2 f_s}{2L_1} = \frac{2f_s^2 \rho_s}{N(\mu_q \rho_q)^{1/2}} \tag{26}$$

This is equivalent to the Sauerbrey equation (eq 1) when N=1.

Example. Figure 6 shows an example of the mass loading effect on the TSM resonator electrical characteristics near resonance for a 6 MHz AT-cut quartz resonator. The curves are the measured response for (a) the unperturbed device and (b) the TSM resonator loaded with 160 nm SiO_2 layer. The primary effect of the mass layer is to translate the admittance curves towards lower frequency without affecting the admittance magnitude. This is consistent with eqs 22 and 23 where there is only an inductive component, L_2, added to the electrical equivalent circuit. This element represents the increased kinetic energy contributed by the mass layer moving synchronously with the resonator surface.

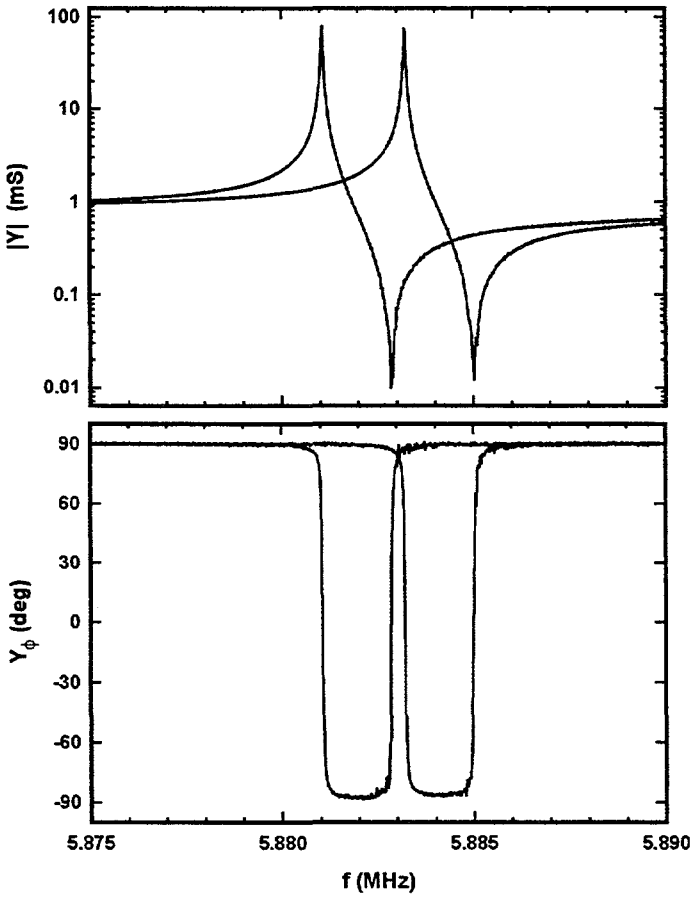

Figure 6. Electrical admittance vs. frequency for a TSM resonator before and after deposition of a 160 nm SiO_2 layer.

Semi-infinite Fluid. When a TSM resonator is operated in a fluid, the shear motion of the crystal surface viscously entrains fluid close to the resonator surface (Figure 7). The velocity field, v_x, generated by this in-plane shear oscillation is determined by solving the Navier-Stokes equation for one-dimensional plane-parallel flow:[23]

$$\eta_l \frac{\partial^2 v_x}{\partial y^2} = \rho_l \dot{v}_x \tag{27}$$

where ρ_l and η_l are the liquid density and shear viscosity, respectively. The solution is

$$v_x(y,t) = v_{xo} e^{-\gamma y} e^{j\omega t} \tag{28}$$

Eq 28 represents a damped shear wave radiated into the fluid by the oscillating device surface. y is the distance from the surface and γ is the complex propagation factor for the acoustic wave:

$$\gamma = \left(\frac{\omega \rho_l}{2\eta_l}\right)^{1/2} (1+j) \tag{29}$$

Substituting eq 29 into eq 28 leads to

$$v_x(y,t) = v_{xo} e^{-y/\delta}\left[\cos\left(\frac{y}{\delta}\right) - j\sin\left(\frac{y}{\delta}\right)\right] e^{j\omega t} \tag{30}$$

where δ is the decay length of the shear wave:

$$\delta = \left(\frac{2\eta_l}{\omega \rho_l}\right)^{1/2} \tag{31}$$

We note that the decay length is related to the kinematic viscosity (η_l/ρ_l) of the fluid.

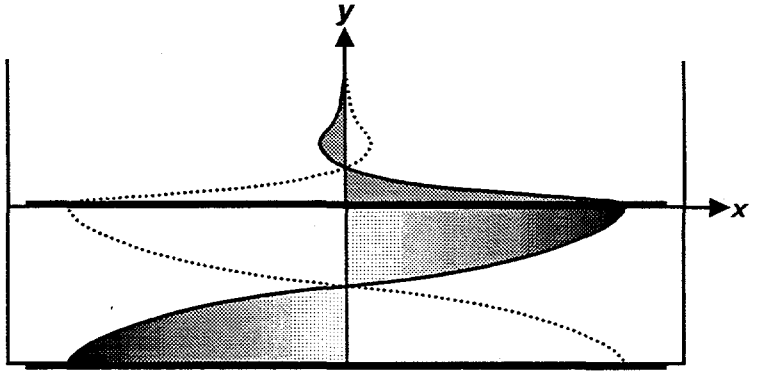

Figure 7. Cross-sectional view of a TSM resonator with a Newtonian fluid on the upper surface.

Newtonian Fluid Case. A Newtonian fluid is one in which the shear stress and the gradient in fluid velocity are related by a constant, independent of amplitude or frequency. The shear stress imposed by the resonator surface on the liquid to generate the velocity field of eq 30 is

$$T_{xy} = -\eta_l \left. \frac{\partial v_x}{\partial y} \right|_{y=0} \tag{32}$$

The surface mechanical impedance contributed by a semi-infinite Newtonian fluid is obtained by combining eqs 3, 30 and 32:

$$Z_s = \left(\frac{\omega \rho_l \eta_l}{2} \right)^{1/2} (1 + j) \tag{33}$$

Combining eqs 15, 16 and 33 gives the motional impedance elements arising from the semi-infinite Newtonian fluid in contact with one surface of the resonator:

$$R_2 \equiv X_2 = \frac{N\pi}{4K^2 \omega_s C_o Z_q} \left(\frac{\omega \rho_l \eta_l}{2} \right)^{1/2} \tag{34}$$

Newtonian liquid loading leads to an equal component of energy storage (X_2) and power dissipation (R_2). The motional reactance, X_2, represents the kinetic energy of the entrained liquid layer and results in a decrease in the frequency of oscillation. The motional resistance, R_2, represents power radiated into the contacting liquid by the oscillating device surface and results in resonance damping.

Example. When liquid contacts one face of the TSM resonator, the electrical response changes, as described by the elements R_2 and X_2. Figure 8 shows admittance vs. frequency data (points) measured as the density-viscosity product ($\rho_l \eta_l$) of a solution contacting the resonator varies. With increasing $\rho_l \eta_l$, the admittance magnitude shows both a translation of the series resonant peak toward lower frequency and a diminution and broadening of the peak. The solid lines in Figure 8 are admittances calculated from the equivalent circuit model when best-fit X_2 and R_2 values are included. The model accurately produces the admittance vs. frequency curves measured under liquid loading using fixed parameters determined from the unloaded resonator. The translation of the admittance curves arises from the reactance contribution, X_2, and the broadening and diminution of the resonance peaks arises from the resistance contribution R_2.

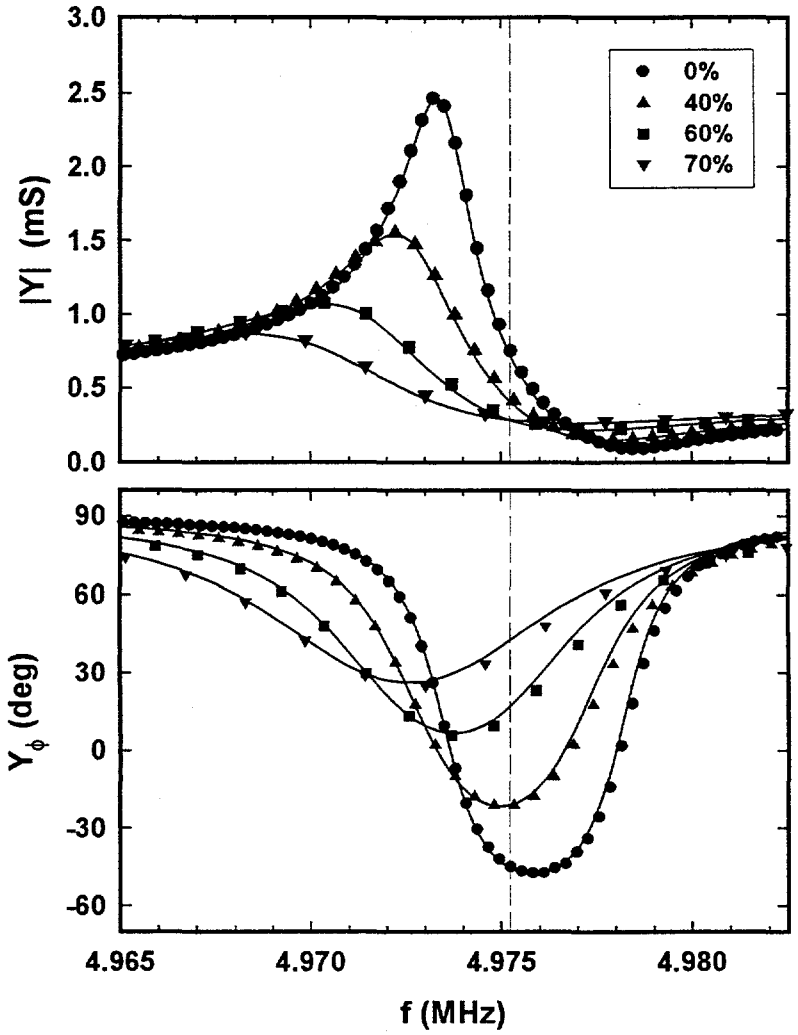

Figure 8. Electrical admittance vs. frequency near the fundamental resonance with glycerol (in water) solutions contacting one side of the TSM resonator. Numbers indicate percentage glycerol. The solid curves are fits to the measured data points.[22]

Similarly, Figure 9 shows the equivalent circuit parameters, R_2 and X_2, as a function of $(\rho_l \eta_l)^{1/2}$ obtained for various glycerol/water solutions. It can be seen that the plot is linear and $R_2 = X_2$, as predicted by eq 34. The best fit from the measured response is extremely close to the predicted response.

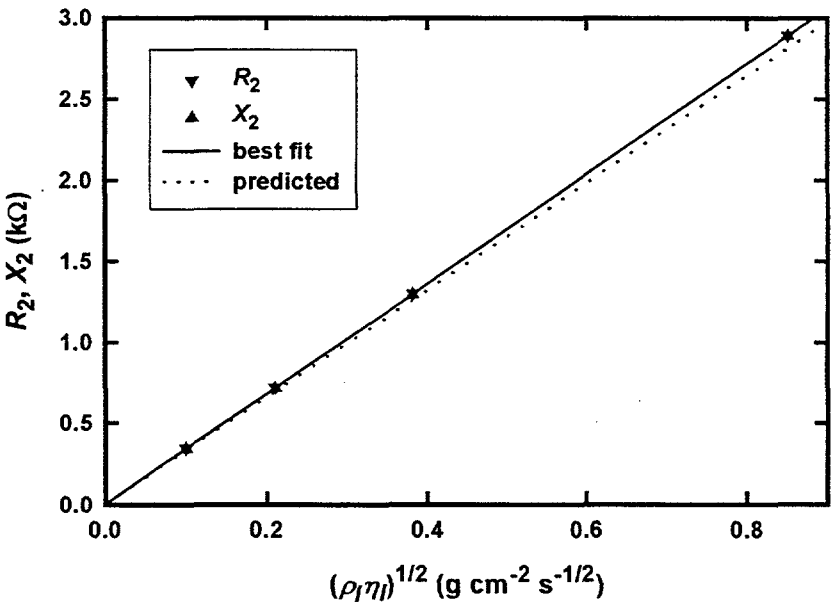

Figure 9. Equivalent circuit parameters (R_2 and X_2) as a function of $(\rho_l \eta_l)^{1/2}$ for glycerol/water solutions which exhibit Newtonian characteristics.

Maxwellian Fluid Case. A Maxwell fluid is one type of non-Newtonian fluid that considers the finite reorientation time of molecules under shear stress. The fluid exhibits a first-order relaxation process:[23]

$$\eta(\omega) = \frac{\eta_0}{1 + j\omega\tau} \tag{35}$$

where η_0 is the low frequency shear viscosity and τ is the relaxation time ($\tau = \eta_0/G_\infty$ where G_∞ is the high frequency rigidity modulus). When the strain rate is low, $\omega\tau \ll 1$, and the Maxwell fluid behaves as a Newtonian fluid. However, when $\omega\tau \approx 1$, unlike Newtonian fluids, the elastic energy cannot be totally dissipated in viscous flow and some is stored elastically. (Also it is interesting to note that when $\omega\tau \gg 1, j\omega\eta = G_\infty$ and the fluid behaves much like a solid.)

Eq 35 can be substituted into eq 32 to give an expression for the shear stress. Then, in a fashion similar to that used for the Newtonian fluid, eqs 35 and 29 are combined to give an expression for the complex propagation factor:

$$\gamma^2 = \frac{j\omega\rho_l}{\eta_0}(1 + j\omega\tau) \tag{36}$$

Eqs 32 and 3 then give an expression for the surface mechanical impedance for a Maxwell fluid:

$$Z_s = \left(\frac{j\omega\rho_l\eta_0}{1+j\omega\tau} \right)^{1/2} \tag{37}$$

Combining eqs 15, 16 and 37 gives the motional impedance elements arising from the semi-infinite Maxwell fluid:

$$R_2 = \frac{N\pi}{4K^2\omega_s C_0 Z_q} \left(\frac{\omega\rho_l\eta_0}{2} \right)^{1/2} \left[1 + \frac{\omega\tau}{\sqrt{1+(\omega\tau)^2}} \right]^{1/2} \left[\frac{1}{\sqrt{1+(\omega\tau)^2}} \right]^{1/2} \tag{38}$$

and

$$X_2 = \frac{N\pi}{4K^2\omega_s C_0 Z_q} \left(\frac{\omega\rho_l\eta_0}{2} \right)^{1/2} \left[1 - \frac{\omega\tau}{\sqrt{1+(\omega\tau)^2}} \right]^{1/2} \left[\frac{1}{\sqrt{1+(\omega\tau)^2}} \right]^{1/2} \tag{39}$$

These statements agree with derivations by Mason in 1965.[25]

It can be seen that when $\omega\tau$ « 1, eqs 38 and 39 reduce to those of a semi-infinite Newtonian fluid (eq 34). When $\omega\tau$ is not negligible, $R_2 > X_2$.

Example. Figure 10 shows the motional impedance parameters computed for fluids with different viscosities showing the influence of molecular reorientation time.

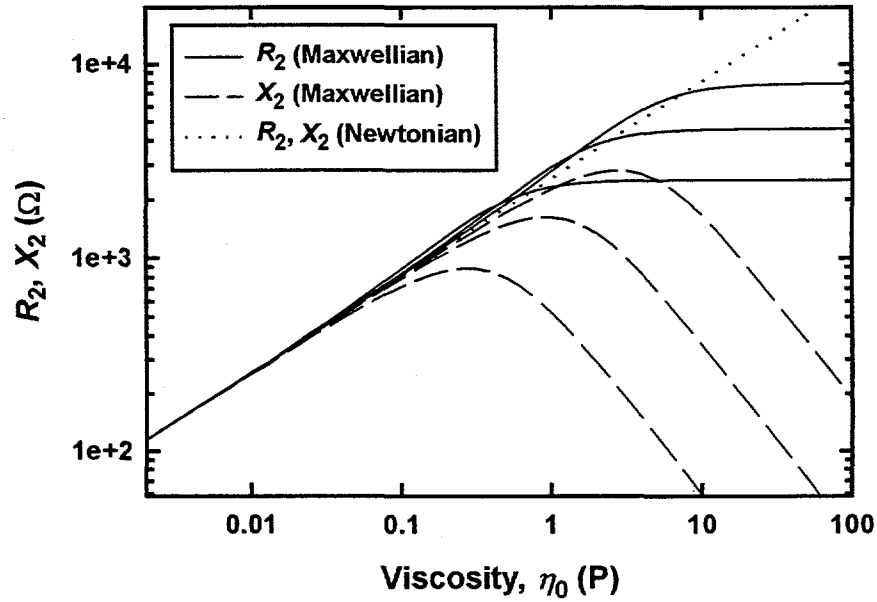

Figure 10. Computed motional impedance parameters (R_2, X_2) for Newtonian and Maxwell fluids as a function of static viscosity and high frequency rigidity modulus: G_∞ = (a) 3×10^7, (b) 1×10^8 and, (c) 3×10^8 dyne cm^{-2}.

At low viscosity ($\eta_0 < 0.1$ P), the fluid response is characteristic of a Newtonian fluid ($R_2 \approx X_2$). However, as η_0 increases, the response deviates from Newtonian behavior, characterized by $R_2 > X_2$, and X_2 eventually decreasing with increasing η_0.

For many materials the relaxation time, τ, and the low frequency viscosity, η_0, are a strong function of temperature. This influences their rheological properties. Figure 11 shows the motional resistance, R_2, and reactance, X_2, measured for a TSM resonator immersed in two different synthetic lubricants. At high temperature, when $\omega\tau \ll 1$, $R_2 \cong X_2$, and both lubricants behave as Newtonian fluids. At low temperature, $R_2 > X_2$ and the lubricants exhibit Maxwell fluid characteristics. The lubricant containing the polymeric additive used as a viscosity enhancer shows significantly more non-Newtonian behavior than the base stock.

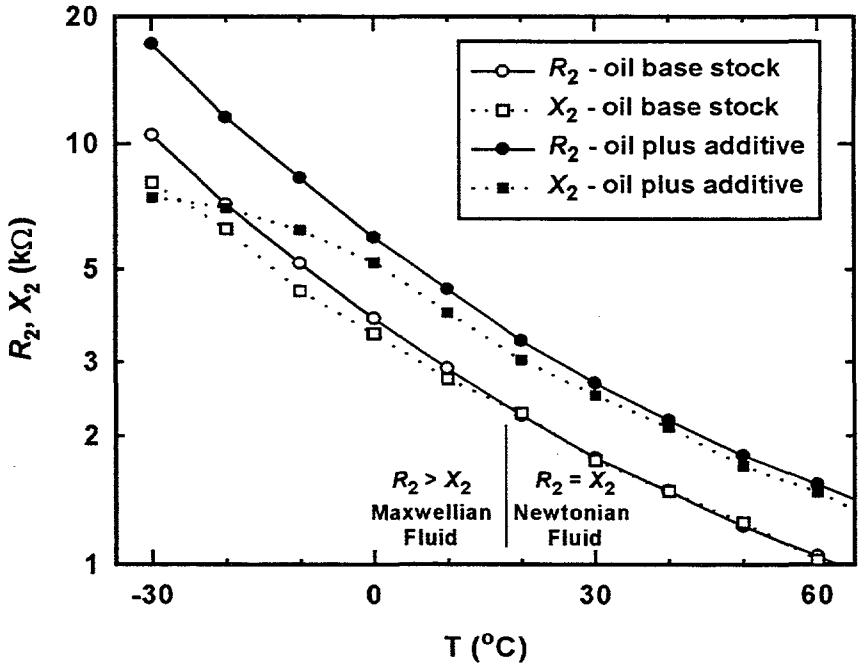

Figure 11. Experimental motional impedance parameters (R_2, X_2) for two synthetic lubricants as a function of temperature.[24]

Viscoelastic Layer: Finite Thickness Case. A finite viscoelastic layer is one with a film thickness smaller than several decay lengths so that the shear acoustic wave generated at the resonator/film interface is reflected at the film/air interface (Figure 12). Therefore, the surface mechanical impedance is dependent upon the phase shift and attenuation of the wave propagating

across the film, i.e., it depends upon the nature of the interference between the waves generated at the lower film surface and those reflected from the upper (film/air) surface.

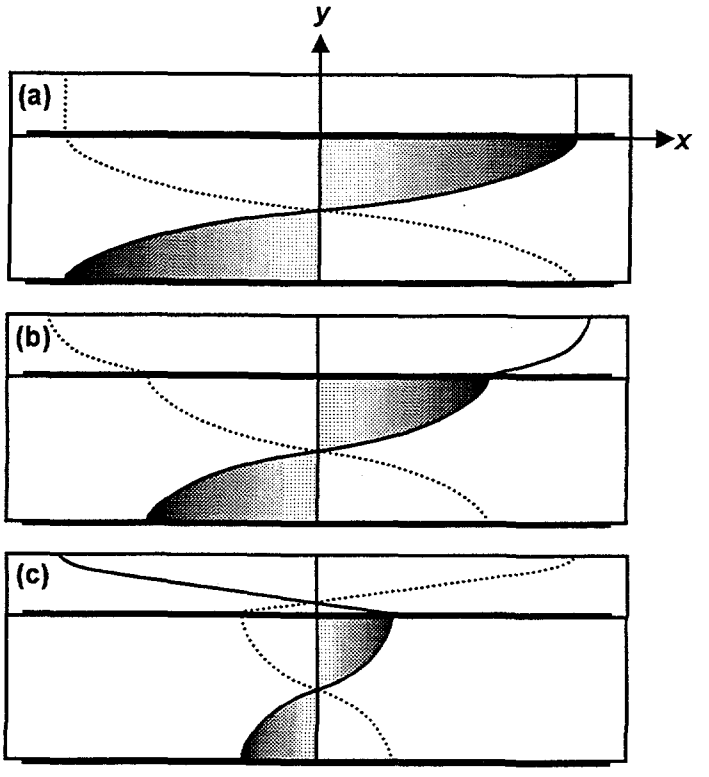

Figure 12. The dynamic film response generated by the oscillating resonator surface varies with the acoustic phase shift, ϕ_f, across the film: (a) for $\phi_f \ll \pi/2$, synchronous motion occurs; (b) for $\phi_f \leq \pi/2$, overshoot of the upper film surface in-phase with the resonator surface occurs (film resonance occurs when $\phi_f = \pi/2$); (c) for $\phi_f > \pi/2$, the upper film surface is 180° out-of-phase. The film is the thin region at the top; the crystal is below. The magnitude of shear displacement in the quartz and the film are scaled to illustrate the differing effects.

Shear displacement in a viscoelastic layer can be described by the equation of motion[17]

$$G\frac{\partial^2 u_x}{\partial y^2} = \rho_f \ddot{u}_x \tag{40}$$

where G is the complex shear modulus ($G = G' + jG''$, where G' is the storage modulus and G'' is the loss modulus) and ρ_f is the film density. This equation can be solved to give the displacement, u_x, in the film as a function of distance from the resonator surface and time. The solution is a superposition of waves propagating in opposite directions due to reflection at the film/air interface:

$$u_x(y,t) = \left(Ae^{-\gamma y} + Be^{\gamma y}\right) \cdot e^{j\omega t} \tag{41}$$

where A and B are constants and γ is the complex wave propagation constant (determined by substituting eq 41 into eq 40):

$$\gamma = j\omega\left(\frac{\rho_f}{G}\right)^{1/2} \tag{42}$$

Two boundary conditions are applied to solve for A and B in eq 41:

(1) $u_x(0) = u_{xo}$ i.e., continuity of particle displacement at the resonator/film interface; and

(2) $T_{xy}(h_f) = 0$ i.e., the upper film surface is stress free.

h_f is the film thickness. After solving for A and B, eq 41 can be written as

$$u_x(y,t) = u_{xo}\left[\frac{e^{\gamma(h_f - y)} + e^{-\gamma(h_f - y)}}{e^{\gamma h_f} + e^{-\gamma h_f}}\right] e^{j\omega t} \tag{43}$$

By substituting expressions for v_x and T_{xy} into eq 3, an expression for the surface mechanical impedance seen at the resonator/film interface is obtained:[11]

$$Z_s = (G\rho_f)^{1/2} \tanh(\gamma h_f) \tag{44}$$

The hyperbolic tangent of the complex argument, γh_f, in eq 44 makes it difficult to separate the load impedance, Z_m[1], into its real and imaginary components, R_2 and X_2, except in a few limiting cases. Thus, it is customary to treat the finite viscoelastic layer as having a single lumped-element complex electrical impedance.

When the phase shift, ϕ_f [ϕ_f = Re(γh_f)], across the film is small, the film's upper surface moves synchronously with the resonator surface (Figure 12a). Since the shear displacement is uniform across the film, no elastic energy is stored or dissipated due to inertial effects. In this regime, the device response is insensitive to G, and only dependent upon the layer mass, ρ_s as described previously. When the phase shift across the film becomes appreciable, the upper film surface lags behind the driven resonator/film interface (Figure 12b). Significant elastic energy is stored and dissipated. In this case, the resonant frequency and damping depend upon film thickness, density, and shear elastic properties.

When $\phi_f = \pi/2$, i.e., the film thickness is one-quarter of the shear wavelength, a resonance effect is created within the film causing maximum coupling of acoustic energy from the TSM resonator to the film. At this point, the interaction between the resonator and film exhibits

characteristics of coupled resonators.[11] Dramatic changes in the motional impedance occur at film resonance due to the enhanced coupling of acoustic energy into the film. Film resonance effects have been recently demonstrated during the electrodeposition of polymer films by varying h_f.[26, 27] Film resonance can also be achieved by varying G or ρ_f (e.g., as they change with temperature).[8, 11] As ϕ_f surpasses $\pi/2$, the upper and lower surfaces go from an in-phase to an out-of-phase condition (Figure 12c).

Example. The change in film dynamics with ϕ_f has a profound effect on device response as exemplified by Figure 13. This shows the admittance magnitude data vs. frequency for a 3 μm trans-polyisoprene film on a 5 MHz TSM resonator operating in the third harmonic as a function of temperature. The shear modulus, G, of the film is altered by varying the temperature, thus allowing ϕ_f to go through $\pi/2$ and exhibit film resonance. Film resonance is indicated by a jump in the admittance peak to higher frequency. Figure 14 shows the corresponding parametric plot (R_2 vs. X_2) for the data of Figure 13 fitted to the lumped element equivalent circuit of Figure 4. Resonance is observed when the conductance reaches a minimum (resonant resistance, R_2, reaches a maximum).

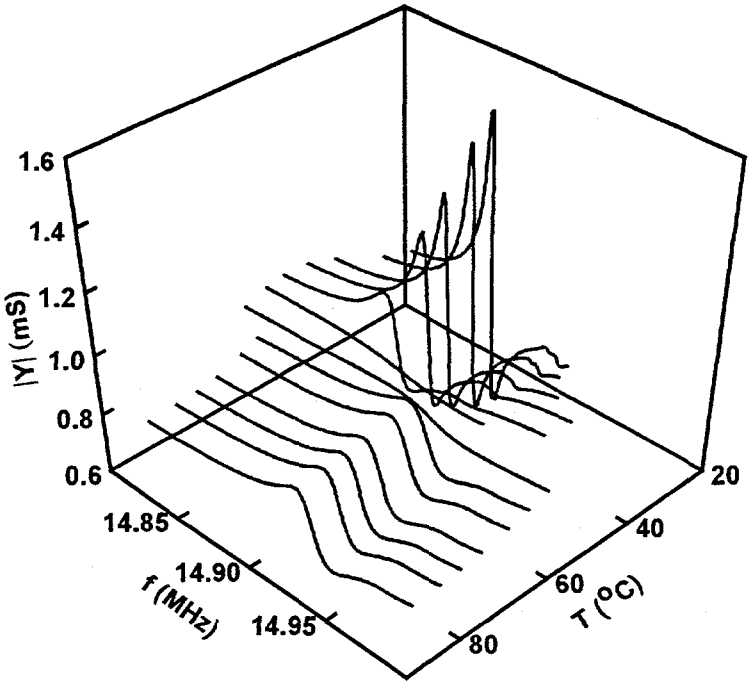

Figure 13. Admittance magnitude vs. frequency as a function of temperature for a 3 μm trans-polyisoprene film on a 5 MHz AT-cut TSM resonator operating in the third harmonic.

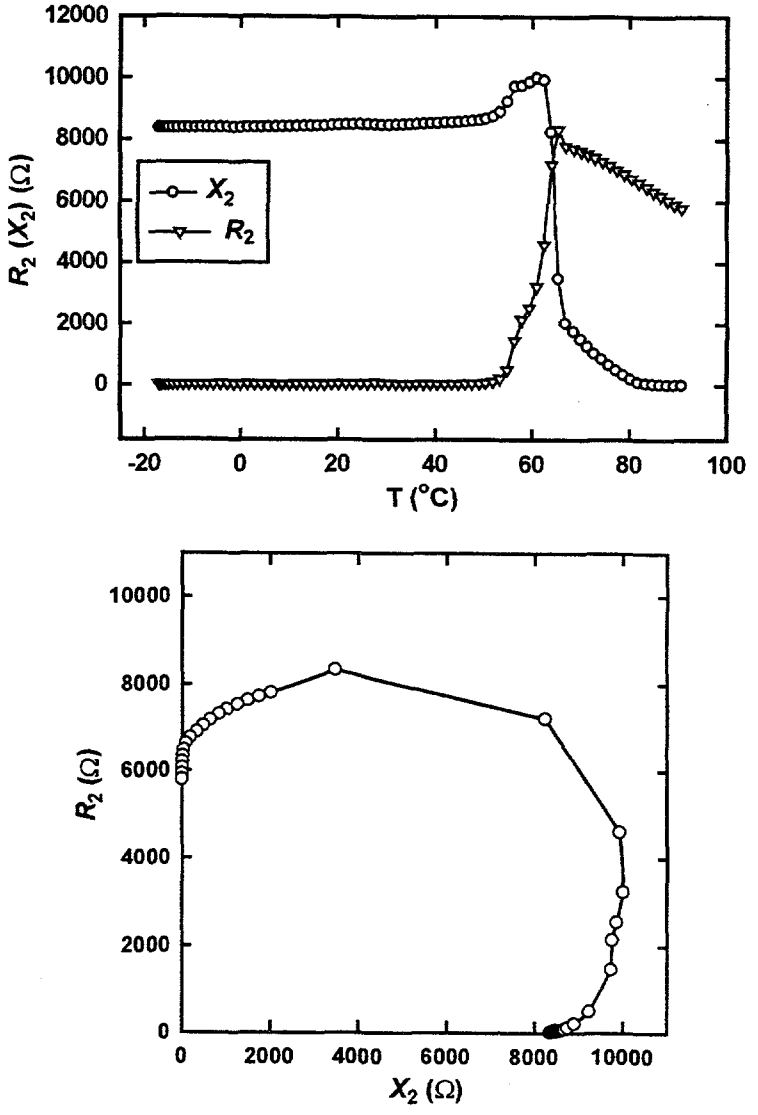

Figure 14. Equivalent circuit parameters (R_2 and X_2) as a function of temperature for the data in Figure 13. The lower plot is a parametric representation of R_2 and X_2.

Viscoelastic Layer: Semi-infinite Case. If the viscoelastic layer is sufficiently thick, or the moduli values are such that the decay length is much smaller than the film thickness, then the film behaves as semi-infinite. Wave propagation in the semi-infinite viscoelastic medium is unidirectional. Therefore, eq 41 can be simplified to

$$u_x(y,t) = u_{xo} e^{-\gamma y} e^{j\omega t} \tag{45}$$

In this limit, the hyperbolic tangent term in eq 44 is equal to one [$\tanh(\gamma h_f) \rightarrow 1$]. The surface mechanical impedance is then represented by

$$Z_s = (G\rho_f)^{1/2} \tag{46}$$

By combining eqs 15, 16 and 46, the equivalent circuit elements can be obtained:

$$R_2 = \frac{N\pi}{4K^2\omega_s C_0 Z_q}\left[\frac{\rho_f(|G| + G')}{2}\right]^{1/2} \tag{47}$$

and

$$L_2 = \frac{N\pi}{4K^2\omega_s^2 C_0 Z_q}\left[\frac{\rho_f(|G| - G')}{2}\right]^{1/2} \tag{48}$$

where $|G| = [(G')^2 + (G'')^2]^{1/2}$. It is possible to invert eqs 47 and 48 so that film storage and loss moduli can be extracted directly from experimentally determined values of R_2 and L_2.

Example. Figure 15 shows the theoretical response for a 10 MHz resonator using the lumped-element model of Figure 4 for a viscoelastic layer where $G' = G'' = 10^7$ dyne cm^{-2} and ρ_f = 1 g cm^{-3}. It can be seen that for thicknesses above 4 μm, the electrical equivalent circuit parameters (R_2 and X_2) are not dependent upon h_f, i.e., the film is behaving as semi-infinite and the TSM resonator is not "seeing" anything beyond this thickness. In this case there would be no reflection at the film/air interface.

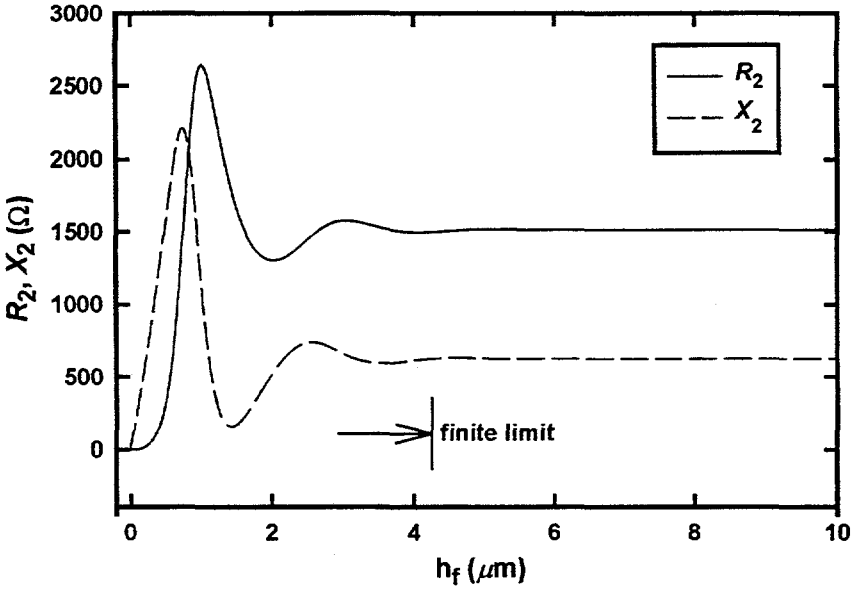

Figure 15. Theoretical equivalent circuit parameters (R_2 and X_2) versus film thickness for a viscoelastic layer where $G' = G'' = 10^7$ dyne cm^{-2} and ρ_f = 1 g cm^{-3}. The film becomes semi-infinite for $h_f > 4$ μm.

Linear Multiple Loading. In general, surface loads on the TSM resonator consisting of multiple combinations of mass layers, liquids and viscoelastic layers cannot be treated in a linear fashion. However, for an ideal mass layer present at the quartz interface, displacement is constant across that layer. Thus, the impedance of a composite, consisting of an ideal mass layer at the resonator surface plus some other perturbation, is the sum of the impedances of both loads considered separately. This is demonstrated for a resonator loaded with an ideal mass layer on the surface with a semi-infinite Newtonian fluid on top.[10, 22] Figure 16 shows the acoustic displacement for a TSM resonator under this loading condition.

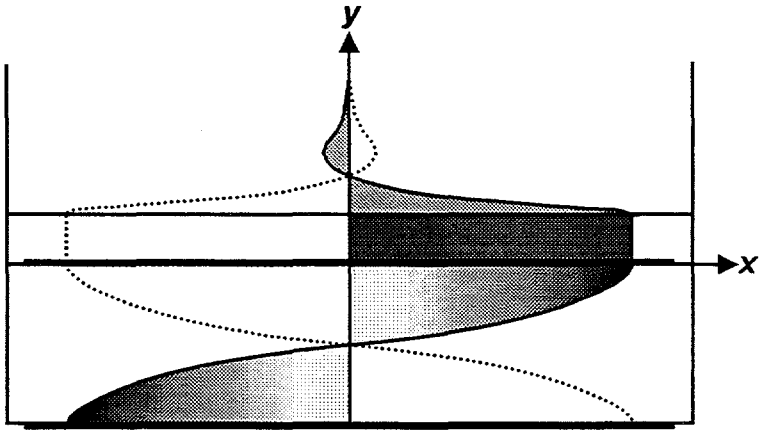

Figure 16. Cross-sectional view of a TSM resonator with an ideal mass layer plus semi-infinite Newtonian fluid on the upper surface.

The surface mechanical impedance is represented by the sum of eqs 21 and 33:

$$Z_s = j\omega\rho_s + \left(\frac{\omega\rho_l\eta_l}{2}\right)^{1/2}(1+j) \tag{49}$$

The equivalent circuit parameters can be extracted as before to give:

$$R_2 = \frac{N\pi}{4K^2\omega_s C_0 Z_q}\left(\frac{\omega_s\rho_l\eta_l}{2}\right)^{1/2} \tag{50}$$

and

$$L_2 = \frac{N\pi}{4K^2\omega_s^2 C_0 Z_q}\left[\left(\frac{\omega_s\rho_l\eta_l}{2}\right)^{1/2} + \omega_s\rho_s\right] \tag{51}$$

From eqs 50 and 51, it can be seen that the addition of the ideal mass layer only affects the inductive component (inertial mass) as expected, while fluid properties affect both inertial mass

and viscous damping equally, as before. Z_m^1 is dependent upon the surface mass density, ρ_s, of the ideal mass layer and the density, ρ_l, and viscosity, η_l, of the liquid. Similarly, solutions can be obtained for resonators loaded with an ideal mass layer plus Maxwell fluid or viscoelastic material (finite or semi-infinite). For simplicity, these solutions are summarized in Table 2.

Example. Figure 17 shows the theoretical responses using the lumped-element model of Figure 4 for a 10 MHz device for (a) an unperturbed resonator, (b) fluid loading only, and (c) an ideal mass layer plus fluid loading. As shown previously, the effect of adding a fluid onto the resonator surface is to decrease the frequency and increase the damping of the spectrum. In addition, the ideal mass layer translates the spectrum towards lower frequency without damping the resonator response. It is possible to separate the physical properties of the two layers due to the linear relationship between the energy storage and power dissipation for a Newtonian fluid. Any excess storage can be attributed to the ideal mass layer.

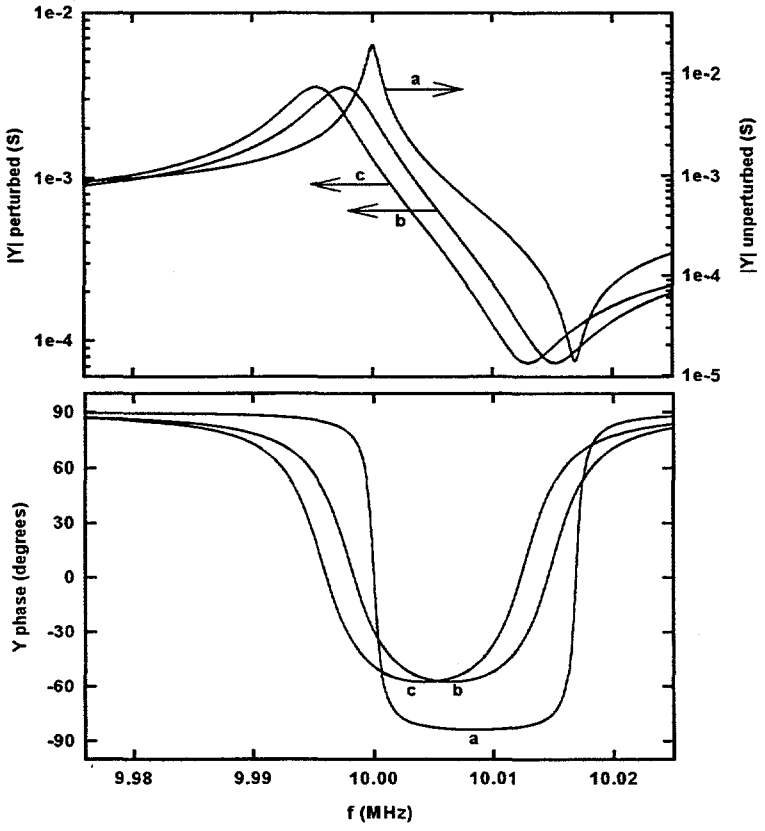

Figure 17. Theoretical admittance response (magnitude and phase) using the lumped-element model of Figure 4 for a 10 MHz TSM resonator: (a) an unperturbed resonator, (b) fluid loading only (c) an ideal mass layer plus fluid loading. ρ_l = 1 g cm^{-3} and η_l = 1 cP.

Non-linear Multiple Loading. In the preceding example, the surface mechanical impedance was the sum of the contributions from the individual layers. In general, multiple layers do not add algebraically, but combine in a non-linear fashion. The simplest and most commonly used example of a non-linear system is that of a finite viscoelastic layer with a Newtonian fluid on top (Figure 18). This is representative of a non-rigid, surface-bound film exposed to a solution. Due to the phase shift across the viscoelastic layer, the total impedance is *not* equal to the sum of the characteristic impedances of the individual layers. Instead the surface mechanical impedance is represented by[14]

$$Z_s = Z_s^{film}\left[\frac{Z_s^{fluid}\cosh(\gamma h_f)+Z_s^{film}\sinh(\gamma h_f)}{Z_s^{film}\cosh(\gamma h_f)+Z_s^{fluid}\sinh(\gamma h_f)}\right] \tag{52}$$

where Z_s^{fluid} is the characteristic mechanical impedance of a Newtonian fluid as described by eq 33; and Z_s^{film} is the characteristic impedance of a viscoelastic film as described by eq 46. The real and imaginary parts of the complex surface impedance are substituted into eqs 15 and 16 to determine equivalent circuit elements (R_2 and X_2). Then Z_m^1 is dependent upon the density, ρ_l, and the viscosity, η_l, of the Newtonian fluid and the shear modulus, G, density, ρ_f, and thickness, h_f, of the viscoelastic film.

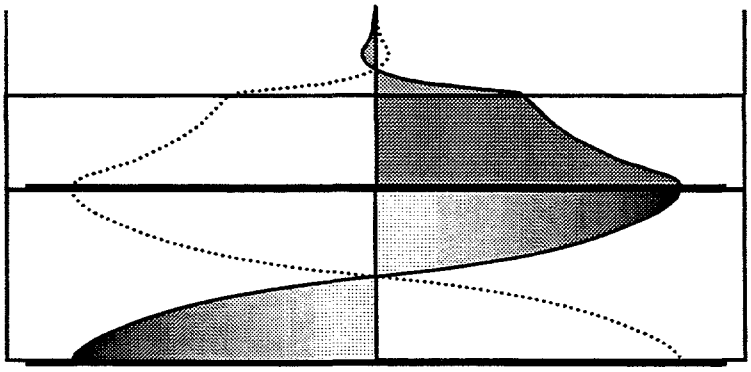

Figure 18. Cross-sectional view of a TSM resonator with a finite viscoelastic layer plus semi-infinite Newtonian fluid on the upper surface.

Eq 52 can be generalized to account for any number of viscoelastic layers on the TSM resonator:[8, 14]

$$Z_s^{(n)} = Z_c^{(n)}\left[\frac{Z_c^{(n+1)}\cosh(\gamma^{(n)}h_f^{(n)})+Z_c^{(n)}\sinh(\gamma^{(n)}h_f^{(n)})}{Z_c^{(n)}\cosh(\gamma^{(n)}h_f^{(n)})+Z_c^{(n+1)}\sinh(\gamma^{(n)}h_f^{(n)})}\right] \tag{53}$$

where $Z_c^{(n)}$ and $Z_c^{(n+1)}$ are the characteristic impedances for the viscoelastic layers as shown in Figure 19 and described by eq 46. The procedure is to stack the layers, starting with a knowledge that the top

(outermost) of the composite resonator is stress free (or in contact with a semi-infinite fluid), and work towards calculating the surface mechanical impedance at the resonator/film interface. This makes it possible to study the effects of many viscoelastic layers on the surface of the TSM resonator, although characterizing or extracting the density, thickness, and shear moduli of the individual layers would be difficult due to the increasing number of parameters. It should be noted that if $Z_c^{(2)} = 0$ in Figure 19, i.e., there is only one viscoelastic layer present, then eq 53 will reduce to eq 44 for a finite viscoelastic layer ($Z_c^{(n+1)} = Z_c^{(2)} = 0$).

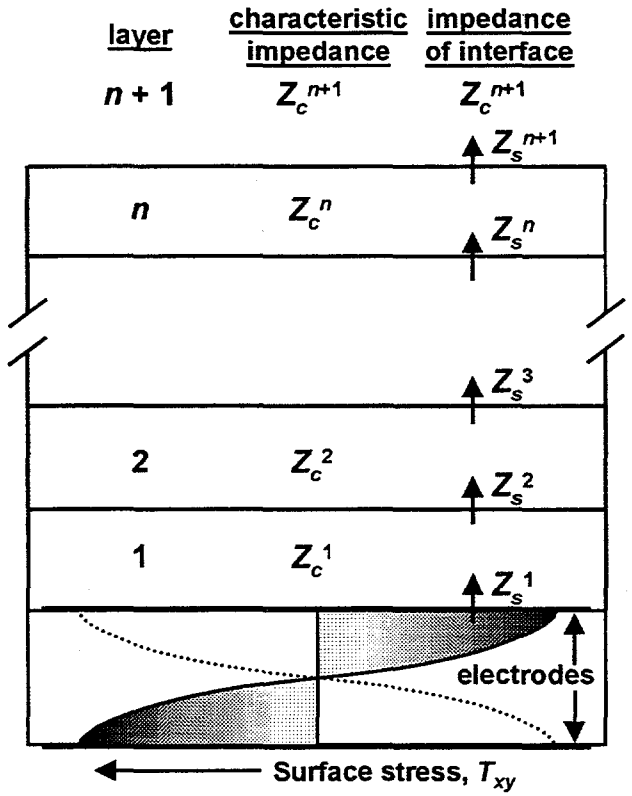

Figure 19. Model for calculating the mechanical impedance imposed on a TSM resonator by multiple viscoelastic layers.

The surface mechanical impedance model given by eq 53 and illustrated in Figure 19 also can be used to represent viscoelastic films with non-homogeneous moduli or density. Such could exist for a polymer film in which a solvent diffuses slowly into the bulk over time; the outer portion of the film is more plastic than polymer near the resonator. In this case, the polymer film can be divided into several segments, each with a graded modulus and density. An effective surface mechanical impedance is then computed. Any layered system of viscoelastic films and fluids (or a system with interspersed mass layers) can be treated with this non-linear model.

Combinations of Linear and Non-linear Loadings. Figure 20 shows the shear displacement of a TSM resonator loaded with three different layers: an ideal mass layer next to the resonator, a viscoelastic layer, and a semi-infinite Newtonian liquid on top. The surface mechanical impedance for this system is simply eq 52 for the viscoelastic layer with liquid overlayer plus the contribution from the ideal mass layer (eq 21). The final expression for Z_s can be extracted from the last entry in Table 2 using $n = 1$ and $Z_c^{(n+1)}$ from eq 33 for a Newtonian liquid. Note here that values of n are assigned only to the layers that contribute to the non-linear loading, and the mass layer is treated separately. Having an expression for Z_s, eqs 15 and 16 are again used to describe the electrical components for the equivalent circuit representation. Z_m^1 is dependent upon the surface mass density, ρ_s, of the ideal mass layer; the shear modulus, G, density, ρ_f, and thickness, h_f, of the viscoelastic film; and the density, ρ_l, and viscosity, η_l, of the Newtonian fluid.

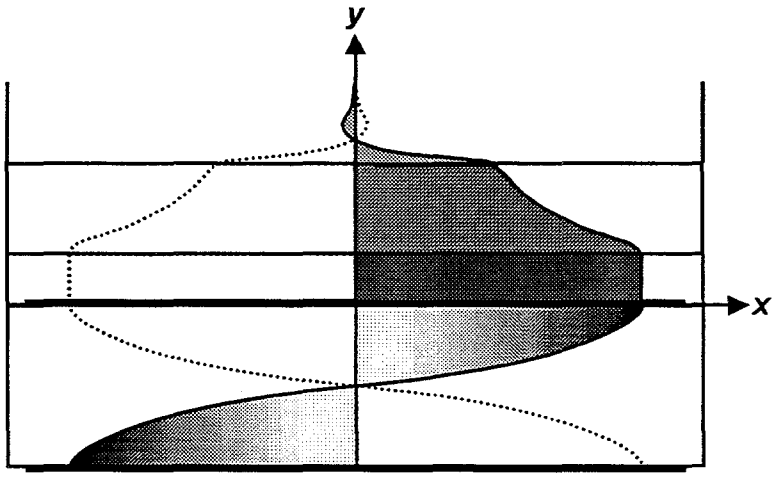

Figure 20. Cross-sectional view of a QCM with an ideal mass layer plus finite viscoelastic layer plus semi-infinite Newtonian fluid on the upper surface.

Example. For this example, we choose to look at the electrochemical deposition of poly(2,2'-bithiophene) (PBT) conducting polymer films onto 10 MHz AT-cut quartz resonators with gold electrodes. This system has been previously studied[7] and by a stepwise process shear moduli values for the polymer film were extracted. The ideal mass layer accounts for any trapped material in surface roughness features (entrapped material moves synchronously with the resonator surface and so can be treated as an ideal mass layer); the fluid represents the deposition solution; and the viscoelastic layer represents the polymer film. The solution used was 5 mmol dm^{-3} bithiophene, 0.1 mol dm^{-3} tetraethylammonium tetrafluoroborate in acetonitrile and the deposition potential, E, was 1.125 V.

Figure 21 shows the crystal impedance spectra acquired dynamically during the course of the deposition process. Upon application of the potential step (E = 0 to 1.125 V), the resonance moves to lower frequency and the peak admittance decreases. This is consistent with the deposition of a film in which there is substantial energy loss, i.e., a viscoelastic PBT film.

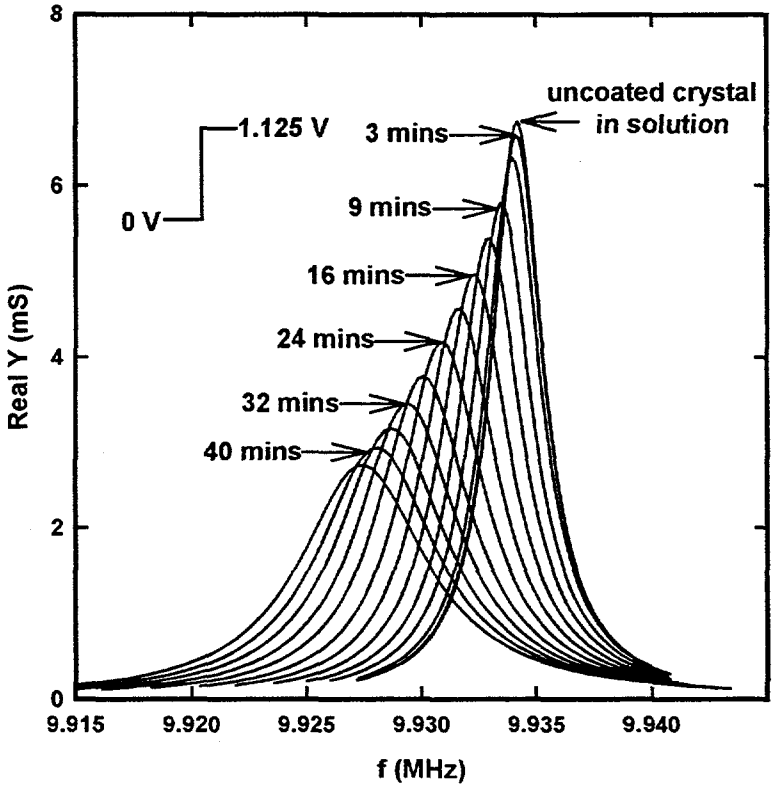

Figure 21. Crystal impedance spectra acquired during the electrodeposition of poly(2,2'-bithiophene). Solution 5 mmol dm^{-3} bithiophene, 0.1 mol dm^{-3} tetraethylammonium tetrafluoroborate, acetonitrile. E = 1.125 V. Numbers indicate time (min) from application of potential step.[7]

This complex three-layer model is of significant value if the parameters of interest (in this case the shear modulus of the film) can be extracted. As can be seen from Table 2, there are many parameters that need to be predetermined in this model in order to extract unique values for the film shear modulus. This can be accomplished in a stepwise manner. First, the deposition solution is characterized so that $\rho_l\eta_l$ and ρ_s are determined as indicated previously for an ideal mass layer in contact with a Newtonian fluid. The values obtained were $\rho_l\eta_l$ = 0.00289 g^2 cm^{-4} s^{-1} (theoretical = 0.00283 g^2 cm^{-4} s^{-1})[28] and ρ_s = 1.03 μg cm^{-2}. Assuming a density of 1 g cm^{-3}, this corresponds to an effective roughness thickness of 10.3 nm. Taking ρ_f = 1 g cm^{-3} and calculating h_f from the charge

passed during deposition, one can now simplify the problem so the only undetermined parameters are G' and G''. Figure 22 shows the resulting G values obtained as a function of deposition time for this system using this model. Extracted moduli are much as expected, starting as a liquid like medium (G'' » G' where $G'' = \omega\eta \approx 2 \times 10^5$ dyne cm^{-2} for this system as indicated on Figure 22) and approaching a rubbery polymer ($G' \approx G''$).

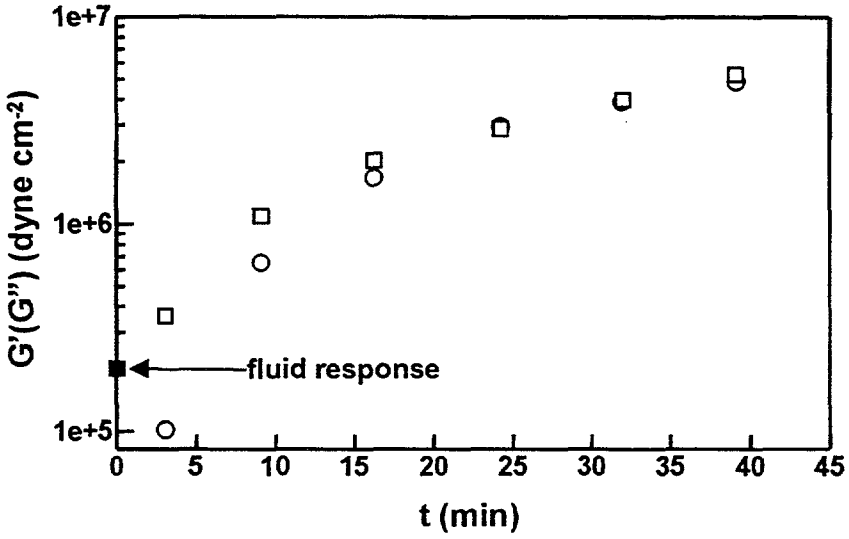

Figure 22. Storage (G',○) and loss (G",□) moduli as a function of deposition time (polymer coverage) computed from the spectral data in Figure 21.

It should be stated that not all mass layers that are part of a multi-layer surface load on a resonator can be treated linearly when determining surface mechanical impedance. The simple linear loading applies only for elastically coupled layers adjacent to the TSM resonator. If a mass layer is interspersed among viscoelastic layers, the stack must be treated non-linearly using eq 53. As a simple example, if a mass layer is deposited on top of a polymer layer, the complete surface mechanical impedance of the two layer system required $Z_c^{(n+1)} = j\omega\rho_s$ to be used. When uncertain about application of linear and non-linear loading contributions, a worthwhile practice is to always treat every layer as a viscoelastic medium using eq 53, and then apply simplifying mathematical constraints.

DISCUSSION

The models we have described offer several aspects of sophistication over and above those previously available. First, they allow one to combine multiple loading elements. This is a necessity for describing any in situ electrochemical experiment, biosensor system, or multi-phase fluid/deposition monitor. Second, it allows smooth transition between finite and semi-infinite films when characterizing a system. This is frequently encountered during a deposition experiment at fixed conditions as the film thickness increases, or during a temperature ramp experiment at fixed film thickness. Third, the expressions for surface mechanical impedance readily lend themselves to diagnostic use. For example, one can explore resonator responses while varying such parameters as film thickness or surface finish, respectively, to distinguish finite vs. semi-infinite behavior, or "surface entrapped" vs. bulk liquid behavior. Fourth, the model provides a relatively transparent link between experimental observations (resonator electrical response) and useful physical parameters intrinsic to the materials used, notably shear moduli and liquid viscosity. This allows study of direct chemical interactions as they relate to mechanical or acoustic characteristics.

We recognize there are certain features and situations that are not covered by the description we offer. First, we have not discussed the case of non-homogeneous layers that are, in one way or another, composites of some sort, e.g., the case of macroscopically porous materials permeated by fluids of (necessarily) very different rheological characteristics. Second, we have not considered in detail the case of spatially inhomogeneous films, whether in terms of structure, density, or viscoelasticity. Third, we have not explicitly described film resonance effects, which have been observed in several polymer systems.[8, 26, 27] Nevertheless, we believe that the generality and simplicity of the model, coupled with the relatively simple diagnostic characteristics associated with the various cases, make it applicable to a wide variety of systems and circumstances encountered in interfacial studies. Further, we envisage subsequent extension, as guided by experiment, to incorporate these more complex situations.

CONCLUSIONS

We have developed an equivalent circuit model describing the surface mechanical impedance of several TSM resonator loads. These include rigidly coupled films and non-rigidly coupled loadings of finite or semi-infinite extent. Important examples of non-rigid loadings include Newtonian or Maxwell fluids and viscoelastic solids, of which polymers are a very important class. The model is capable of converting measured electrical impedance data through surface mechanical impedance to materials properties, such as viscosity, density, and shear modulus. In the case of finite loading elements, film thickness may also be determined.

The model is extended to a range of multi-element loadings, which may be linear or non-linear dependent upon the materials involved and location of layers. Specifically, we develop expressions for two-layer loadings, such as a rigid film with a liquid overlayer and a finite viscoelastic film with liquid overlayer, and for three-layer loadings, such as a rigid layer with a finite viscoelastic overlayer and a liquid above that. However, we also demonstrate the general procedure for resonator loading with an arbitrary number of rheologically distinct overlayers.

For the cases explored, we provide many experimental examples from diverse interfacial structures and processes involving a wide range of materials. The success of the model in handling these physically diverse cases suggests its general utility.

ACKNOWLEDGEMENTS

The authors thank Kent Pfeifer for his careful review of the paper. HLB thanks the University of Leicester, UK for a University Research Studentship. Sandia is a multiprogram laboratory operated by Sandia Corporation, a Lockheed Martin Company, for the United States Department of Energy under Contract DE-AC04-94AL85000.

SUMMARY

Surface Perturbation	Physical Example	Surface Mechanical Impedance (Z_s)	Variable Parameters
unperturbed	air	0	-
ideal mass layer	Sol-gel film	$j\omega\rho_s$	ρ_s
semi-infinite Newtonian fluid	water	$\left(\frac{\omega\rho_l\eta_l}{2}\right)^{1/2}(1+j)$	ρ_l, η_l
semi-infinite Maxwell fluid	High viscosity liquids	$\left(\frac{j\omega\rho_l\eta_0}{1+j\omega\tau}\right)^{1/2}$	ρ_l, η_0, τ
semi-infinite viscoelastic layer	thick polymer film	$(G\rho_f)^{1/2}$	G', G'', ρ_f
finite viscoelastic film	thin polymer film	$(G\rho_f)^{1/2}\tanh(\gamma h_f)$	G', G'', ρ_f, h_f
ideal mass layer + semi-infinite Newtonian fluid	electrochemical deposition of Ag	$j\omega\rho_s+\left(\frac{\omega\rho_l\eta_l}{2}\right)^{1/2}(1+j)$	ρ_s, ρ_l, η_l
ideal mass layer + semi-infinite Maxwell fluid	oil on an unpolished surface	$j\omega\rho_s+\left(\frac{j\omega\rho_l\eta_0}{1+j\omega\tau}\right)^{1/2}$	ρ_s, ρ_l, η_0, τ
ideal mass layer + semi-infinite viscoelastic layer	thick polymer film on an unpolished surface	$j\omega\rho_s+(G\rho_f)^{1/2}$	ρ_s, G', G'', ρ_f
ideal mass layer + finite viscoelastic layer	thin polymer film on an unpolished surface	$j\omega\rho_s+(G\rho_f)^{1/2}\tanh(\gamma h_f)$	ρ_s, G', G'', ρ_f, h_f
Multiple viscoelastic layers	electrochemical deposition of a thin polymer film	$Z_c^{(n)}\left[\frac{Z_c^{(n+1)}\cosh(\gamma^{(n)}h_f^{(n)})+Z_c^{(n)}\sinh(\gamma^{(n)}h_f^{(n)})}{Z_c^{(n)}\cosh(\gamma^{(n)}h_f^{(n)})+Z_c^{(n+1)}\sinh(\gamma^{(n)}h_f^{(n)})}\right]$	G', G'', ρ_f, h_f, ρ_l, η_l
ideal mass layer + multiple viscoelastic layers	electrochemical deposition of a thin polymer film on an unpolished surface	$j\omega\rho_s+Z_c^{(n)}\left[\frac{Z_c^{(n+1)}\cosh(\gamma^{(n)}h_f^{(n)})+Z_c^{(n)}\sinh(\gamma^{(n)}h_f^{(n)})}{Z_c^{(n)}\cosh(\gamma^{(n)}h_f^{(n)})+Z_c^{(n+1)}\sinh(\gamma^{(n)}h_f^{(n)})}\right]$	ρ_s, G', G'', ρ_f, h_f, ρ_l, η_l

Table 2. Summary of surface mechanical impedance (Z_s) for various loading conditions on the TSM resonator

NOMENCLATURE

A	effective electrode area (cm^2)
A, B	constants
C: C_1; C_0; C_p; C_0^*	capacitance (F): motional contribution from unperturbed resonator; static; parasitic; sum of static and parasitic
f: f_0; f_s	frequency (Hz): unperturbed fundamental; series resonant
G: G'; G''; G_∞; $G^{(n)}$	shear modulus (dyne cm^{-2}): storage; loss; high frequency rigidity modulus; shear modulus of n^{th} layer
h: h_q; h_f; h_s; $h_f^{(n)}$	thickness (cm): quartz; film; ideal mass layer; n^{th} layer
j	$\sqrt{-1}$
K^2	electromechanical coupling coefficient
L: L_1; L_2	motional inductance (H): unperturbed resonator; surface perturbation
Δm	areal mass density (g cm^{-2})
N	harmonic number
N'	transformer turn ratio representing the quartz electromechanical coupling
R: R_1; R_2	motional resistance (Ω): unperturbed resonator; surface perturbation
S_{11}	reflection scattering parameter
t	time (s)
T_{xy}	sinusoidal steady-state shear stress in the x-direction on a y-normal plane (Nm^{-2})
u_x: u_{xo}	x-component of displacement (cm): at y=0
v: v_q; v_x; v_{xo}	velocity (m s^{-1}): acoustic velocity in quartz; x-directed shear particle velocity; x-directed shear particle velocity at y=0
X	reactance of the quartz piezoelectric interaction (Ω)
X_2	surface load reactance (Ω)
Y	admittance (S)
Z: Z_0; Z_q; Z_{AB}; Z_{CD}; Z_s;	impedance (Ω): characteristic impedance of measurement system (typically 50 Ω); quartz characteristic impedance; complex electrical input impedance; complex mechanical impedance; surface mechanical impedance
Z_m: Z_m^0; Z_m^1	motional impedance (Ω): unperturbed resonator; surface perturbation

$Z_c^{(n)}$; Z_n	characteristic impedance of n^{th} layer (Ω); surface mechanical impedance seen by n^{th} layer
τ	molecular relaxation time (s)
ω: ω_s	angular frequency ($2\pi f$) (Hz): series resonant ($2\pi f_s$)
δ	decay length (cm)
ρ: ρ_f; ρ_{iml}; ρ_l; ρ_q; $\rho_f^{(n)}$	density (g cm^{-3}): film; ideal mass layer; liquid; quartz; n^{th} layer
ρ_s	surface mass density (g cm^{-2})
ε_q	dielectric permittivity of quartz (A^2 s^4 g^{-1} cm^{-3})
γ: $\gamma^{(n)}$	complex propagation factor: of n^{th} layer
η: η_l; η_q; η_0	shear viscosity (g cm^{-1} s^{-1}): liquid; quartz effective; low frequency
ϕ: ϕ_q; ϕ_f	phase angle (Radians): quartz; film
μ_q	quartz shear elastic constant (dyne cm^{-2})

REFERENCES

(1) *Interactions of Acoustic Waves with Thin Films and Interfaces*, The Royal Society of Chemistry, London, *Faraday Discuss.* **1997,** *107*

(2) Sauerbrey, G. *Z. Phys.* **1959,** *155*, 206-222.

(3) Nomura, T.; Minemura, A. *Nippon Kagaku Kaishi* **1980**, 1261.

(4) Kanazawa, K. K.; Melroy, O. R. *IBM J. Research and Development* **1993,** *37*, 157-171.

(5) Buttry, D. A. In *Electroanalytical Chemistry*, Ed. Bard, A. J, Marcel Dekker: New York, **1991**; vol. 17, pp. 1-85.

(6) Oyama, N.; Ohsaka, T. *Prog. Polymer Sci.* **1995,** *20*, 761-818.

(7) Bandey, H. L.; Hillman, A. R.; Brown, M. J.; Martin, S. J. *Faraday Discuss.* **1997,** *107*, 105-121.

(8) Lucklum, R.; Behling, C.; Cernosek, R. W.; Martin, S. J. *J. Phys. D-Appl. Phys.* **1997,** *30*, 346-356.

(9) Lucklum, R.; Hauptmann, P. *Faraday Discuss.* **1997,** *107*, 123-140.

(10) Martin, S. J.; Granstaff, V. E.; Frye, G. C. *Anal. Chem.* **1991,** *63*, 2272-2281.

(11) Martin, S. J.; Frye, G. C. *Ultrason. Symp.* **1991**, 393-398.

(12) Martin, S. J.; Wessendorf, K. O.; Gebert, C. T.; Frye, G. C.; Cernosek, R. W.; Casaus, L.; Mitchell, M. A. *IEEE Freq. Cont. Symp.* Salt Lake City, UT, USA. **1993**, 603-608

(13) Martin, S. J.; Frye, G. C.; Wessendorf, K. O. *Sens. Actuators A* **1994,** *44*, 209-218.

(14) Granstaff, V. E.; Martin, S. J. *J. Appl. Phys.* **1994,** *75*, 1319-1329.

(15) Martin, S. J.; Frye, G. C.; Senturia, S. D. *Anal. Chem.* **1994,** *66*, 2201-2219.

(16) Bandey, H. L.; Gonsalves, M.; Hillman, A. R.; Glidle, A.; Bruckenstein, S. *J. Electroanal. Chem.* **1996,** *410*, 219-227.

(17) Rosenbaum, J. F. *Bulk Acoustic Wave Theory and Devices*; Artech House: Boston, **1988**.

(18) Christopoulos, C. *The Transmission-Line Modeling Method*; Oxford: University Press,**1995**.

(19) Cernosek, R. W.; Martin, S. J.; Hillman, A. R.; Bandey, H. L. *IEEE Trans. Ultrasonics, Ferroelectrics and Freq. Cont.* **1998,** *45*, 1399-1407.

(20) Krimholz, R.; Leedom, D. A.; Mathaei, G. L. *Electrochem. Lett.* **1970,** *6*, 137-44.

(21) Ballato, A.; Bertoni, H. L.; Tamir, T. *IEEE Trans. Microwave Theory Tech.* **1974,** *MTT-22*, 14-25.

(22) Martin, S. J.; Frye, G. C.; Ricco, A. J.; Senturia, S. D. *Anal. Chem.* **1993,** *65*, 2910-2922.

(23) White, F. M. *Viscous Fluid Flow*; New York: McGraw Hill, **1991**.

(24) Martin, S. J.; Cernosek, R. W.; Spates, J. J. *Digest, 8th Int'l. Conf. on Solid-State Sens. and Act. and Eurosens. IX,* Stockholm, Sweden **1995,** 712-715.

(25) Mason, W.P. *Physical Acoustics, Volume II-Part A*; New York: Academic Press, **1965.**

(26) Saraswathi, R.; Hillman, A. R.; Martin, S. J. *J. Electroanal. Chem.* in press.

(27) Hillman, A.R.; Brown M.J.; Martin, S.J. *J. Am. Chem. Soc.*, in press.

(28) *The Handbook of Chemistry and Physics*, 75th ed.; C.R.C. Press: Florida, **1994**.